Abteilung MN
Gymnasium Kirchenfeld
Oktober 2014

Modeling and Fabrication of a Multilayer Stack for a Nanoparticle-Enhanced UV Filter

Luc Schnell

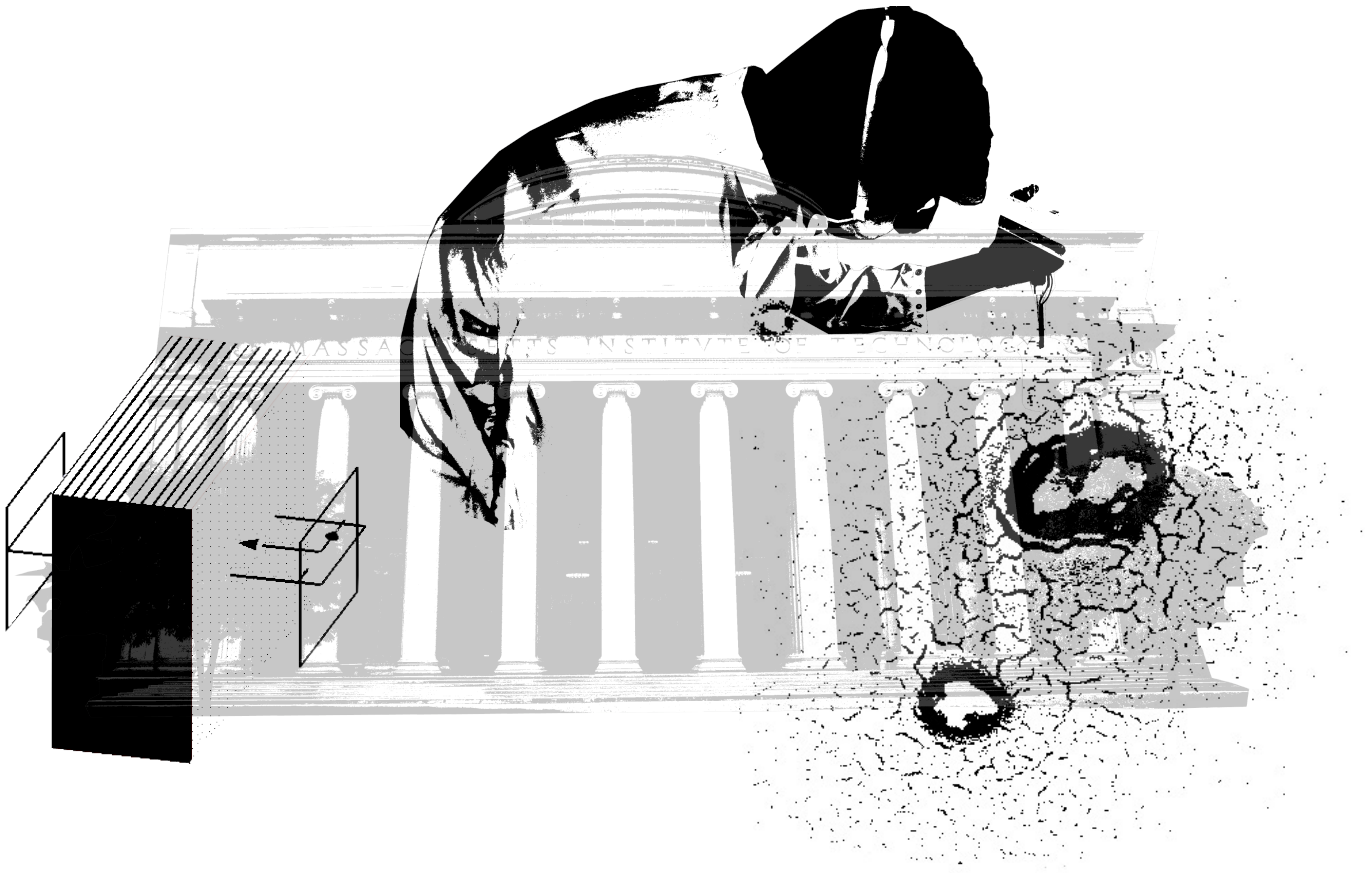

Entstanden während dem Research Science Institute am MIT
Department of Materials Science and Engineering

Betreut durch Dr. Christoph Rytz

Inhaltsverzeichnis

I Vorwort

Diese Arbeit ist im Rahmen des Research Science Institute (RSI), organisiert durch den Center for Excellence in Education (CEE), am Massachusetts Institute of Technology (MIT) entstanden. Dabei verbrachte ich gemeinsam mit 82 anderen Gymnasiastinnen und Gymnasiasten aus der ganzen Welt sechs Wochen auf dem MIT Campus und erhielt einen Einblick in die aktuelle Forschung auf höchstem Niveau. Das RSI findet jedes Jahr statt und ist ein Wissenschafts-Förderprogramm für begabte Gymnasiastinnen und Gymnasiasten in den Vereinigten Staaten. Zu den nationalen Schülern werden jährlich rund 30 internationale Schülerinnen und Schüler aufgenommen, zu denen ich dieses Jahr dazugehören durfte. Das Kernstück des RSI-Programms ist eine eigene wissenschaftliche Arbeit in einem Forschungsteam an einer der Universitäten in Boston. Dazu kommen in der ersten Woche und an zahlreichen Abenden Vorlesungen von MIT Professorinnen und Professoren, aktuellen Forscherinnen und Forschern und sogar Nobelpreisträgern, welche die RSI Schülerinnen und Schüler besuchen dürfen.

Am Ende der ersten Woche lernte ich mein Forschungsteam und meine Mentoren kennen, die mir beim Ausführen des eigenen wissenschaftlichen Projektes zur Seite stehen sollten. Ausgehend von meinen Interessen für die Physik hatten die Organisatoren des RSI ein Forschungsteam für Optik am MIT Department for Materials Science and Engineering (DMSE) für mich ausgesucht. Die genaue Fragestellung wurde von meinen Mentoren aus dem Forschungsteam bestimmt. Ich sollte eine Machbarkeitsstudie für die Entwicklung eines mit Aluminium-Nanopartikeln verbesserten UV-Filters durchführen. Dieser sollte nur das Spektrum der elektromagnetischen Strahlung im Solar Blind, also im Wellenlängenbereich, der von der oberen Atmosphäre absorbiert wird und die Erdoberfläche nicht erreicht, durchlassen. Von der zweiten bis zur fünften RSI Woche brachte ich erst meine Kenntnisse auf den nötigen Stand, um die Aufgabe überhaupt verstehen zu können und führte dann eine theoretische sowie eine praktische Studie für den UV-Filter durch. Während dieser Zeit wurde ich von meinen Mentoren unterstützt, war aber häufig auch auf mich allein gestellt und musste eigene Lösungswege finden, da die Mentoren gleichzeitig auch ihre eigenen Forschungsarbeiten voran trieben. In der letzten Woche schrieb ich meine Forschungsergebnisse in der vorliegenden Arbeit nieder und präsentierte sie in einem Kurzvortrag vor der RSI Gesellschaft und meinem Forschungsteam.

Modeling and Fabrication of a Multilayer Stack for a Nanoparticle-Enhanced UV Filter

Luc Schnell

under the direction of
Mr. Corentin Monmeyran, Mr. Brian Pearson, Dr. Anuradha Agarwal
and Prof. Lionel C. Kimerling

Electronic Materials Research Group
MIT Department of Materials Science and Engineering

Research Science Institute
July 30, 2014

Abstract

The thicknesses and refractive indices of alternating dielectric and aluminum layers in a multilayer stack for a short-wave UVC filter must be designed to allow only for the desired wavelengths to be transmitted. The parameters were optimized in a computational model using transfer-matrix and Finite Difference Time Domain (FDTD) methods, in order for the filter to have a peak transmission >15% at 200 nm and an out-of-band transmission $<10^{-9}$% for the whole visible and infrared spectrum. The extinction ratio can be increased by inserting aluminum nanoparticles in the dielectric layers. In this study, a UV filter suitable for many applications working in the solar blind spectrum was modeled. Further, in a practical feasibility study, the creation of the dielectric layers with inserted nanoparticles for the filter was assessed. It was discovered that it was difficult to obtain uniform layers, with evenly distributed nanoparticles, using these methods.

Summary

A UV filter can be created by designing the thicknesses and optical properties of thin layers of two alternating materials in a stack. Since light traveling through this stack can be reflected several times at the layer boundaries, there are many different paths it can take. The sum of all light exiting the filter on the other side equals the total light transmitted. With a computational model, a filter suitable for many UV light applications was found in this study. In a practical feasibility test, the layers of the first material with small aluminum particles added were created and their structure analyzed under the electron microscope.

1 Introduction

The part of the short-wave UVC radiation from 200 nm to 280 nm is strongly absorbed by the ozone layer, resulting in an absence of this spectrum on earth's surface. This is called the solar blind spectrum [1]. UV filters that have their peak transmission in this selective range can be used for UV non-line-of-sight short-range communication, such that a signal originating from the transmitter is scattered by particles in the atmosphere and can then be detected by the receiver without requiring a direct line of sight. This is possible due to low background radiation in the solar blind [2]. Further applications for these filters include astronomy and UV spectroscopy, where information about a sample or a celestial body can be obtained by measuring the amount of UV light absorbed by its particles [3].

Currently, there are UV filters on the market with a peak transmissivity in the solar blind spectrum, but there are none that are inexpensive, can be domestically produced, integrate well in existing systems, have wide acceptance angles, have high out-of-band suppression, and have high peak transmissivity simultaneously. These properties are important for the applications stated above. Currently used filters for the solar blind range have in-band peak transmissions up to 10% and out-of-band transmissions $< 10^{-10}$% from 300 nm to 770 nm and $< 2{\times}10^{-4}$% from 770 nm to 1,100 nm [2].

The solar blind UV filter designed in this study should have a peak transmissivity > 15% at 200 nm, an out-of-band transmission $<10^{-9}$% for the whole visible and infrared spectrum and an extinction ratio $> 10^9$ at the upper boundary of the solar blind, which is given by the ratio of the higher transmission level at 200 nm (signal) to the lower level at 290 nm (background radiation). The sharp drop in transmission is needed, because the longer wavelengths are not completely blocked by the ozone layer and therefore no longer belonging to the solar blind. The widely-used structure of the filter is a multilayer stack consisting of several thin silicon dioxide and/or titanium dioxide layers separated by aluminum layers. Incident light

is partly transmitted and partly reflected at the material interfaces, taking many different pathways in the filter before exiting the multilayer stack (see Figure 1). By designing the thicknesses and the refractive indices of the layers in the right way, only the light rays of the desired range of wavelengths, after having taken different pathways through the filter, interfere constructively on the exit side, thus leading to high transmission.

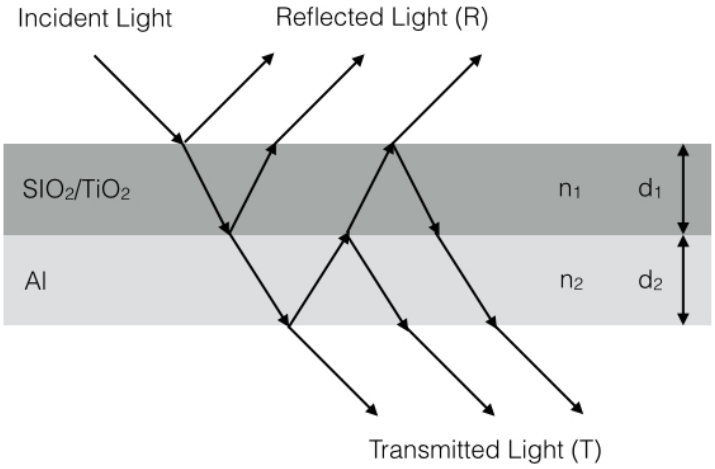

Figure 1: Two layers of the stack with refractive indices n_1,n_2 and thicknesses d_1, d_2 are displayed. The arrows show some of the different pathways for incident light. The total transmitted light (T) is given by the radiation of the different pathways interfering with themselves when exiting the filter on the side of the aluminum layer. This applies analogously for the total reflected light (R) on the opposite side.

The high extinction ratio at the upper boundary of the solar blind can be achieved by adding nanoparticles with a diameter of ∼40 nm into the stack. When excited by radiation with a wavelength of around 280 nm (upper boundary of the solar blind), the electrons in the nanoparticles oscillate with their natural resonant frequency. With this resonance condition the amplitude of the oscillating electrons is higher, therefore enhancing light absorption and scattering at around 280 nm.

In this paper, we investigate the structure of the multilayer stack. First, a theoretical study applying the transfer-matrix method was performed to model ideal refractive indices, thick-

nesses and numbers of layer pairs in the multilayer stack using MatLab. The stack with the best parameters found in MatLab was then modeled even more realistically using a Finite Difference Time Domain (FDTD) method Lumerical. In a practical feasibility study thin films consisting of the dielectric materials for the filter were created with sol-gel and spin coating methods. Aluminum nanoparticles were added to the precursors of these layers. With the electron microscope and the profilometer, the structure of the layers and the inserted nanoparticles was analyzed. The aim of the practical study was to create uniform layers with evenly distributed nanoparticles for the filter.

2 Modeling of the Multilayer Stack

2.1 Materials and Methods

2.1.1 Calculating Transmission

The transfer-matrix method used in this study is an algorithm for reflectivity and transmission calculations of multilayer structures [4]. A matrix was calculated for every part of the multilayer stack that alters the amplitude or phase of an electromagnetic wave. Two types of matrices were used. The transfer matrix accounts for the change in amplitude at a material interface, while the propagation matrix accounts for the phase change and absorption of light by passing through a layer. By multiplying all the propagation and transfer matrices of the individual layers, the total inverse transfer matrix for the filter can be found. The total inverse transfer matrix relates the amplitude of the light on the incidence side of the filter to the amplitude on the exit side, thus containing information about the transmission and reflection of light by the stack. A multilayer stack with n pairs of aluminum and dielectric layers was investigated (see Figure 2).

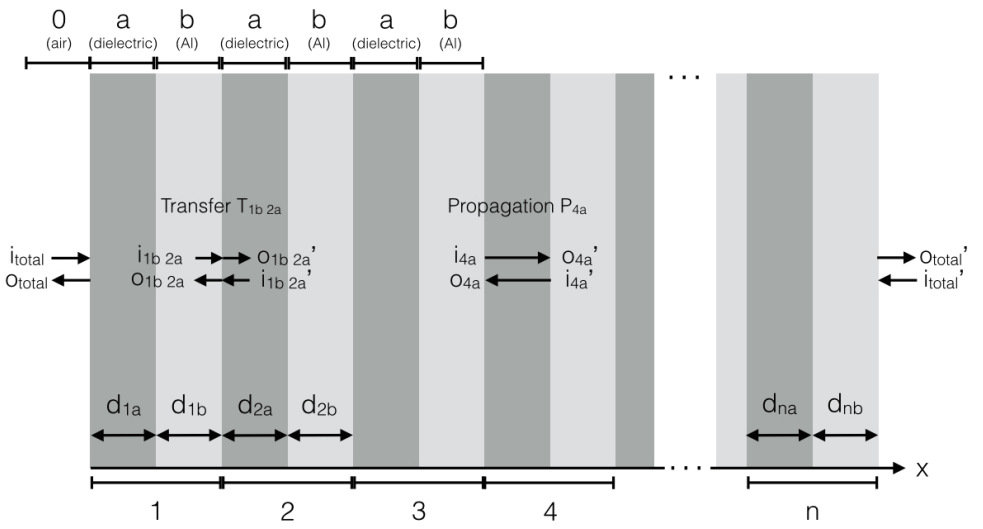

Figure 2: Graphical representation of the multilayer stack. It consists of n pairs of a dielectric and an aluminum layer with (complex) refractive indices n_a, n_b and thicknesses d_{ia}, d_{ib}. A transfer and a propagation matrix with the incident light-waves i, i' (input) and the exiting light-waves o, o' (output) are shown.

The unified refractive index of the dielectric layers is denoted n_a, the different thicknesses as d_{ia}. A lossless propagation of electromagnetic radiation (no absorption) in the dielectric layers was assumed. The refractive index for aluminum as a function of the wavelength of the radiation was obtained from a refractive index database [5]. It includes the complex component $i\kappa$, which accounts for the absorption in the material. The complex refractive index $\tilde{n}$ for aluminum is given by $\tilde{n} = n + i\kappa$. The thicknesses of the layers are denoted as d_{ib}.

The change in amplitude of radiation due to a transition from material 1 to material 2 with (complex) refractive indices n_1,n_2 can be found using the transfer matrix T_{12} (see Figure 2) [6, 7]:

$$\begin{pmatrix} o'_{12} \\ i'_{12} \end{pmatrix} = T_{12} \begin{pmatrix} i_{12} \\ o_{12} \end{pmatrix} = \frac{1}{2n_2} \begin{pmatrix} n_1 + n_2 & n_2 - n_1 \\ n_2 - n_1 & n_1 + n_2 \end{pmatrix} \begin{pmatrix} i_{12} \\ o_{12} \end{pmatrix}. \tag{1}$$

The propagation matrix, P_1, accounts for the absorption and the phase change of light traveling through a layer 1 with (complex) refractive index n_1 and a thickness d_1. The phase change depends on the wavelength λ of the radiation. Since the light-waves o and i travel in opposite directions, the exponents in the matrix have opposite signs (see Figure 2) [6]:

$$\begin{pmatrix} o_1' \\ i_1' \end{pmatrix} = P_1 \begin{pmatrix} i_1 \\ o_1 \end{pmatrix} = \begin{pmatrix} e^{\frac{i2\pi d_1 n_1}{\lambda}} & 0 \\ 0 & e^{-\frac{i2\pi d_1 n_1}{\lambda}} \end{pmatrix} \begin{pmatrix} i_1 \\ o_1 \end{pmatrix}. \tag{2}$$

The total inverse transfer matrix that relates the amplitude of the radiation output of the filter with that of the input can be found by multiplying all of the individual transfer and propagation matrices for each layer [4]:

$$T_{total}^{-1} = T_{01a} P_{1a} T_{1a1b} P_{1b} T_{1b2a} ... T_{nanb} P_{nb} T_{nb0} = \begin{pmatrix} M_{11} & M_{12} \\ M_{21} & M_{22} \end{pmatrix}. \tag{3}$$

Finally, the transmission T and the reflection R for the multilayer stack can be found from the following expressions [4]:

$$T = \left| \frac{1}{M_{11}} \right|^2 \qquad R = \left| \frac{M_{21}}{M_{11}} \right|^2 . \tag{4}$$

We chose the calculation with the total inverse transfer matrix to avoid unnecessary divisions of large numbers resulting in computation rounding errors due to an insufficient number of significant digits.

2.1.2 Parameter Optimization

Values for the parameters number of layer pairs, n, refractive index for the dielectric layers, n_a, and thicknesses of the layers, d_{ij}, were optimized to match the desirable filter properties using MatLab code that ran a loop for a predetermined number of times. In a first simulation,

a unified thickness d_1 for all dielectric layers and a unified thickness d_2 for all aluminum layers were assumed. In each loop of the MatLab code, the transmission for the wavelengths from 150 nm to 2,000 nm was calculated based on the randomly generated parameters n, n_a, d_1 and d_2 within the ranges stated in Table 1.

Range	Layer pairs n ∈ N	Refractive index n_a	Thickness d_1[nm]	Thickness d_2[nm]
min	1	1.7	0	0
max	20	1.9	100	100

Table 1: Ranges for the parameters of the multilayer stack (unified thicknesses).

The limit for the number of pairs of layers, n, was set at 20, since the fabrication of more than 40 layers would be too costly. The range for n_a corresponds to the refractive indices approachable with aluminium dioxide and titanium dioxide layers. The maximum for the thicknesses d_1, d_2 was set at 100 nm, since multilayer structures generally only operate with thicknesses being a small fraction of the wavelengths they are designed for ($\lambda = 200$ nm in this study).

The properties of the transmission curve were analyzed by MatLab at the end of each loop. First, the basic requirements for a curve to be further assessed were a transmission greater than 15% for the wavelength at 200 nm as given in the design specifications and a transmission smaller than 0.001% for 300 nm to have a drop in transmission around 280 nm (upper boundary of the solar blind). Since the resulting curves had high transmissions in the visible and infrared spectra, the basic requirement at 200 nm had to be lowered to a transmission greater than 10%. For the curves that met the basic requirements, the total area under the curve from 300 nm to 2,000 nm (the integral) was calculated. The other curves were discarded. The program returned the 10 curves with the smallest area and their corresponding parameters after completing the defined number of loops.

To achieve the desired peak transmission > 15% at 200 nm, a multilayer stack with different thicknesses d_{ij} for each layer was investigated based on the results of the study with unified thicknesses. This time the basic requirements for the curve were a transmission >15% at 200 nm and a transmission <0.001% at 300 nm. Again the integral of the transmission curve from 300 to 2,000 nm was to be minimized. The number of layer pairs was fixed at 13, as given in the parameters for the best curve found in the study with uniform thicknesses. The ranges for the other parameters are listed in Table 2. The ranges for the thicknesses d_{ia}, d_{ib} could be defined more strictly than before, based on the values of the optimized thicknesses d_1, d_2 found in the study with uniform thicknesses.

Range	Refractive index n_a	Thickness d_{ia}[nm]	Thickness d_{ib}[nm]
min	1.7	29	8
max	1.9	49	18

Table 2: Ranges for the parameters of the mulitlayer stack (different thicknesses).

2.1.3 Modeling with Lumerical

The multilayer stack with the best parameters found in MatLab was modeled using a software called Lumerical, to verify the results calculated with the transfer-matrix method. Lumerical is based on the FDTD method. Using the light source as the origin, Lumerical calculates the electric field by solving Maxwell's equations for every point in a grid system. Given the condition of an infinitessimally small grid, the model would accurately reflect reality. The best multilayer stack was modeled in Lumerical in 3D (see Figure 3).

A plane wave was chosen as light source. The monitor measuring the electric field transmitted by the filter was placed behind the filter. For the measurement of the reflection, a second monitor on the same side as the source was added to the simulation. The electric field was then calculated in a plane normal to the layers of the filter, resulting in a much lower

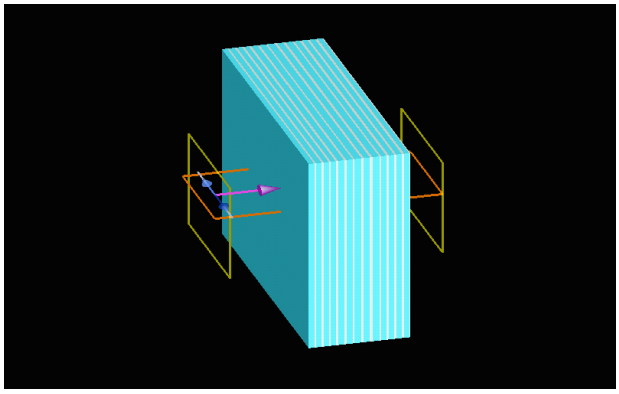

Figure 3: The multilayer stack modeled in Lumerical. The dielectric (blue) and aluminum (gray) layers are displayed. The monitors (yellow) measure the electric field on both sides of the filter. The light source (purple) lies in the plane, where the electric field is calculated (orange).

computation time than for a 3D calculation. This transformation is appropriate as long as the rays of light entering the filter are parallel, only interfering thereby with other light rays in a plane normal to the layers of the stack. The highest accuracy for the grid in Lumerical was chosen. To investigate the influence of variations in the layer thicknesses and the incidence angle of light on the transmisson, the dimensions of the layers and the propagating direction of the plane wave were changed.

2.2 Results

2.2.1 Unified Thicknesses

10^6 loops were performed by the MatLab program to compute the ideal parameters for a multilayer stack with unified thicknesses. The 10 graphs with the smallest integral of the transmission curve from 300 nm to 2,000 nm are given in Table 3.

Despite the very large range of possible values for the thicknesses and the number of layer pairs, the optimized parameters did not deviate significantly. The ranges amounted to 8.4 nm for d_1, 4.2 nm for d_2 and 4 for n. Only the values for n_a covered most of the defined range from 1.7 to 1.9.

Number	Refractive index n_a	Thickness d_1	Thickness d_2	Number of layer pairs n
1	1.71	39.3 nm	13.8 nm	13
2	1.70	41.1 nm	14.1 nm	12
3	1.78	39.0 nm	13.2 nm	15
4	1.78	39.0 nm	13.2 nm	15
5	1.73	39.0 nm	12.0 nm	16
6	1.71	39.3 nm	13.4 nm	13
7	1.76	33.0 nm	11.9 nm	14
8	1.78	38.6 nm	15.0 nm	12
9	1.71	32.7 nm	10.8 nm	15
10	1.83	36.7 nm	13.58 nm	14

Table 3: The 10 best sets of parameters for the unified thicknesses calculated by MatLab.

2.2.2 Different Thicknesses

The set of parameters for a filter with different thicknesses for each layer with the smallest area under the transmission curve from 300 nm to 2,000 nm was calculated in MatLab. The refractive index n_a is 1.75 and the number of layer pairs n is 13. The thicknesses d_{ia}, d_{ib} are listed in Table 4.

i	1	2	3	4	5	6	7	8	9	10	11	12	13
d_{ia} [nm]	36.1	37.7	34.0	31.7	41.0	42.2	47.6	40.0	45.5	34.9	35.0	35.7	32.1
d_{ib} [nm]	10.9	13.4	13.8	14.9	14.2	10.6	15.2	15.9	12.0	16.8	14.1	15.9	8.5

Table 4: The thicknesses of the dielectric layers, d_{ia}, and the thicknesses for aluminum layers, d_{ib}, for the optimized set of parameters.

The curve for the transmission and reflection of a multilayer stack with these parameters calculated is shown in Figure 4. According to the data obtained from Lumerical the peak transmission is 19.7% at 200 nm. For visible and infrared light an average transmission of 1.6×10^{-10}% with a standard deviation of 4.2×10^{-10} is given. The reflection curve shows low values at 200 nm. The reflection of the undesired wavelengths is generally very high with an average of 84.1% with standard deviation of 13.5 for visible and infrared light.

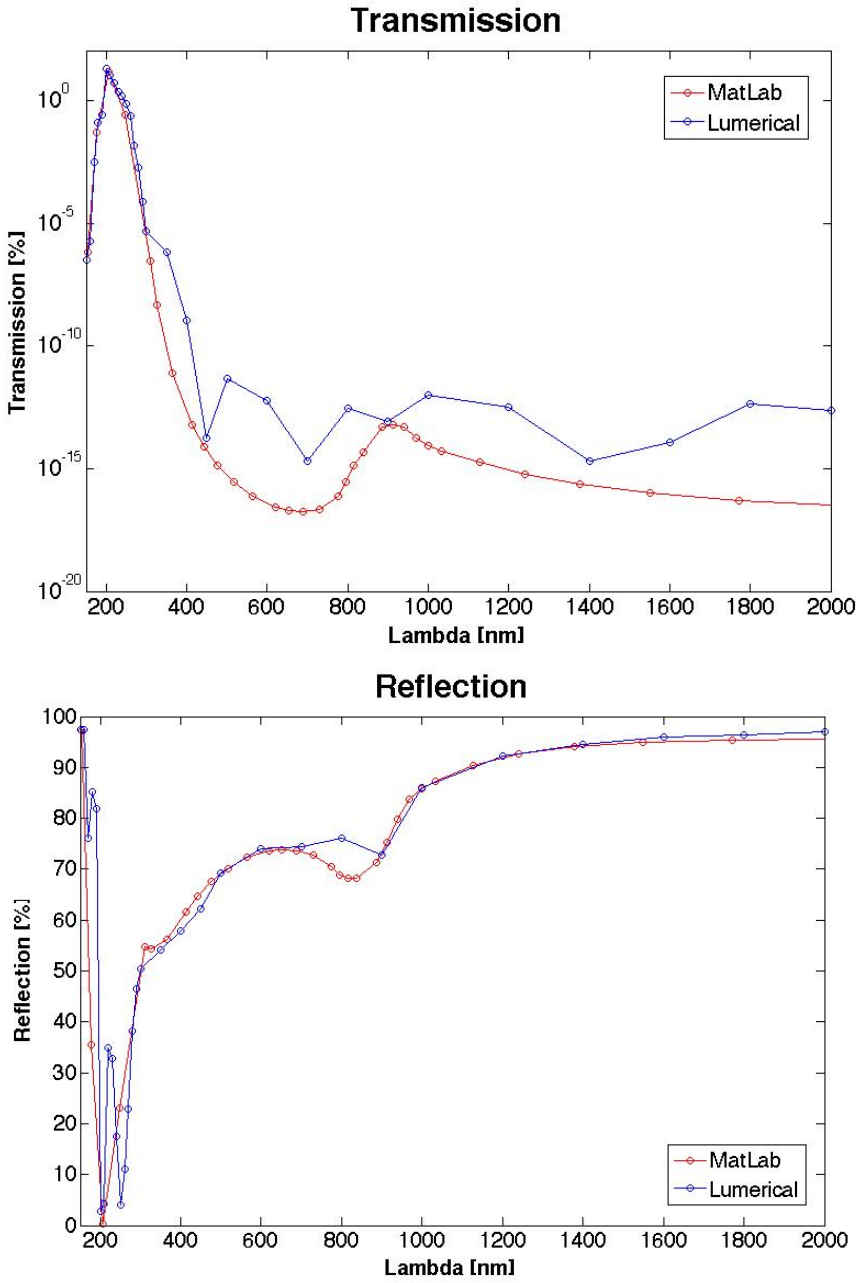

Figure 4: Transmission and reflection of the light spectrum for the best set of parameters. The red lines show the values calculated in MatLab. The blue curves are the values for the same stack modeled in Lumerical. Note that a logarithimic scale was applied for transmission, while the axis scale for reflection is linear. Some of the intensity of the incoming light is lost due to absorption (the sum of the transmission and the reflection is therefore not equal to 100%). This fact was taken into account with the complex refractive indices. The nanoparticle enhancement, however, is not considered in this model.

2.2.3 Angle of Incidence

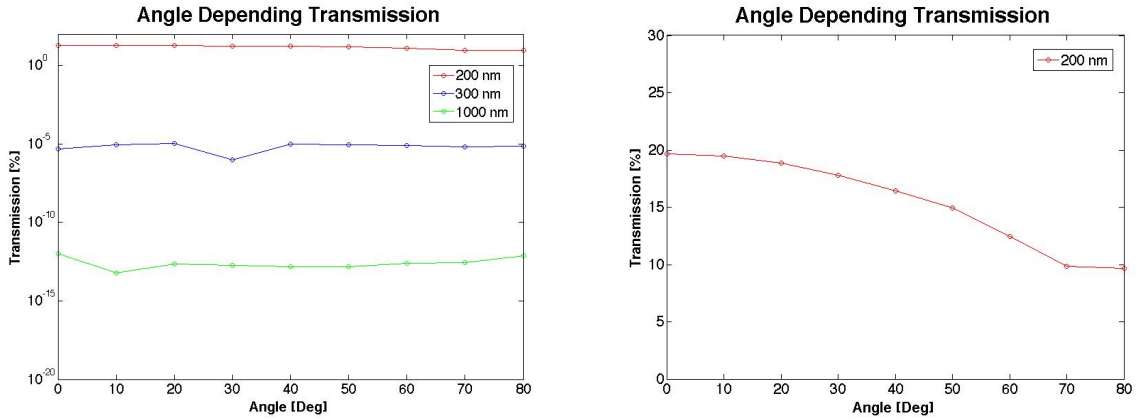

Figure 5: Effect of the angle of incidence on the transmission of different wavelengths. For the diagram on the left a logarithmic scale for the transmission was chosen. The right diagram shows the transmission of 200 nm more closely in a linear scale.

The effect of the angle of incidence on the transmission of different wavelengths is shown in Figure 5. On a logarithmic scale, the transmission of the wavelengths does not change significantly by varying the angle of incidence of the plane wave. However, a decrease in the transmission from 19.7% to 9.7% at high angles of incidence can be observed by looking closer at the curve for 200 nm.

2.2.4 Transmission Variation

Graphs showing the effect of variations in the thicknesses of the layers in the multilayer stack are given in Figure 6. An overall trend for the wavelengths from 300 nm to 2,000 nm cannot be stated, but the transmission stays low ($<10^{-10}$%). Around 200 nm however, an increase in the thicknesses of the layers has a significant effect on the transmission. With an increase of 1 nm for the thicknesses of all layers, the transmission at 200 nm is decreased from 19.7% to 3.8%, pushing the filter out of design specifications. By further increasing the thicknesses to additional 2 nm, the transmission drops to 0.2%.

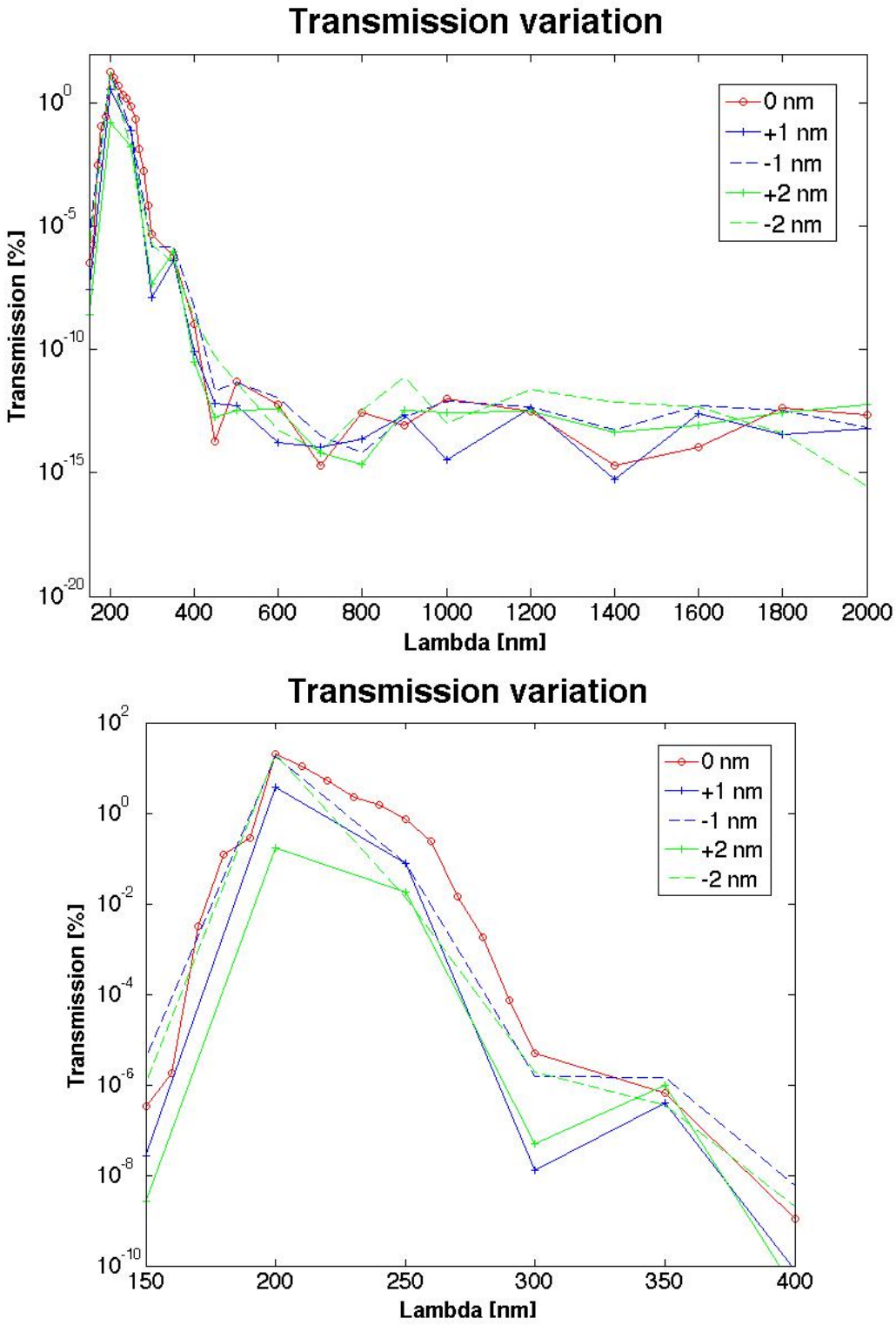

Figure 6: The effects of variations in the thicknesses of the layers on the transmission. The lower diagram shows the decrease in the peak transmission at 200 nm in closer detail.

3 Xerogel Thin Films

3.1 Materials and Methods

3.1.1 Fabrication of Thin Films

Sample	Solvent	Additive	Precursor	Catalyst
1	13 mL ethanol	—	5 mL TEOS	200 μL ammonia sol. 640 μL water
2	20.2 ml ethanol	—	1 mL titanium isopropoxide	—
3	20 mL ethanol	—	1 mL titanium isopropoxide	—
4	commercial sol.	15 mg Al nanoparticles	—	—
5	commercial sol.	30 mg Al nanoparticles	—	—

Table 5: Volumes of the reactants for the different samples.

The sol-gel and spin coating processes allow for the creation of very thin but uniform dielectric layers. The advantages of this method include a low deposition temperature (in this study the samples were deposited at room temperature) and a low overall cost [8]. The sol-gel process started with a liquid, called the sol, that consisted of all reagents. These included a methoxyde, containing the metal atoms for the ceramic layer (silica or titanium), an alcohol (the solvent), a small amount of water (which is a catalyst), and, depending on the reaction, a further base or acid catalyst. During the sol-gel process, the methoxy molecules reacted with the water in the alcohol, thereby becoming hydrolyzed [9]. The hydrolyzed molecules formed large polymers through condensation reactions, converting the initial sol into a gel. The speed of the condensation reaction affects the structural properties of the final layer. Spin coating was then used to obtain a uniform distribution of the gel on a wafer substrate. In the spin coater, the wafer was rotated at high speeds and the gel driven outward by the centrifugal force, so that it became evenly spread out over the wafer due to surface tension.

Due to its high relative surface area and the formation of more polymers through reaction with water in the air, evaporation and further gelling took place and the gel became a solid called xerogel on the wafer. By heating up this xerogel, the uniformity of its structure may be increased.

The precursors for the sol-gel process were mixed in a 50mL Erlenmeyer flask. The volumes of the reagents are given in Table 5. After adding the chemicals, the Erlenmeyer was placed on a hot-plate magnetic-stirrer device, letting the sol becoming a gel during the time and at the temperature stated in Table 6. A commercial sol-gel solution was added to the first trial, since the spin coating did not succeed at first.

Sample	Temperature	Time
1	50°C	90 min
2	50°C	15 min
3	room temp.	15 min
4	room temp.	15 min
5	room temp.	15 min

Table 6: Temperature and time parameters for gelification of the samples.

The stirring speed for all trials was 400 rpm. After the time stated above, the sample was then taken to the spin coater. The Erlenmeyer flask was covered with parafilm to avoid water in the air affecting the reaction. All samples were spin coated at a speed of 2,000 rpm for 20-30 s. Samples 1 and 2 were then cleaved into smaller parts with a scribe. These parts were either left as they were, annealed on the hot plate or annealed in the vacuum-oven. The annealing procedures for Samples 1 and 2 are given in Table 7.

Sample	Annealing
1.1	not annealed
1.2	oven, 200°C
2.1	not annealed
2.2	hot plate, 200°C

Table 7: Annealing Procedures for Samples 1 and 2.

3.1.2 Analysis of Samples

The fabricated samples were analyzed with the profilometer and the scanning electron microscope (SEM). A crack was made in the xerogel layer with a razor blade without damaging the silicon wafer below. The profilometer could then measure the thickness of the xerogel layer by moving its needle over the crack. The roughness R_a found by the profilometer states the arithmetic average of the surface deviating from the ideal position [10]. SEM analysis was also performed under 800 to 20,000 times magnification.

3.2 Results

3.2.1 Silicon dioxide

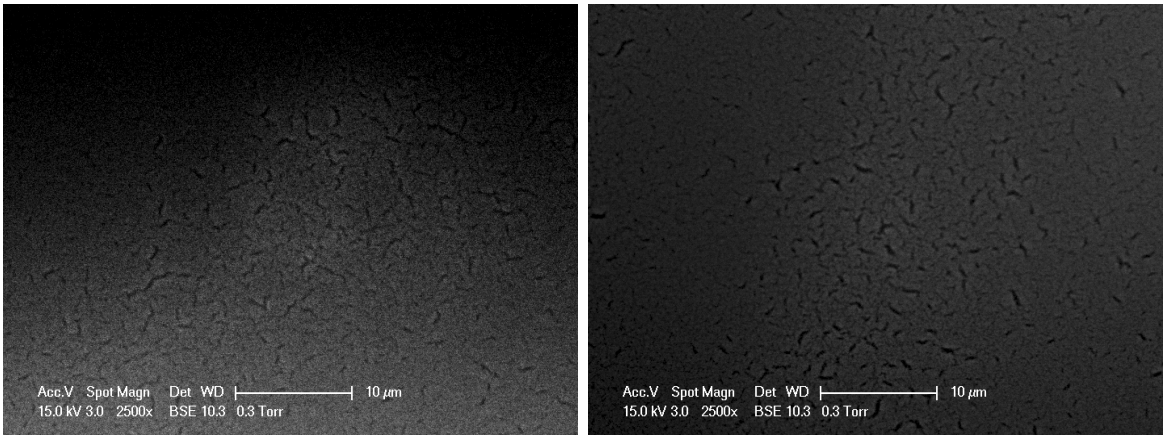

(a) Not annealed. (b) Vacuum oven at 200 °C for 2 h.

Figure 7: SEM pictures of the silicon dioxide layers for Samples 1.1 and 1.2. The sample on the right was annealed after the spin coating process.

Figure 7a shows the silicon dioxide layer of Sample 1.1 at a magnification of 2,500× under the SEM. This sample was not annealed after the sol-gel process. Cracks with a length of about $2 - 4$ μm can be seen in the layer. The R_a roughness of the layer found with the profilometer was 3.8 ± 0.1 nm. The thickness of the layer measured with the scratch in the dielectric layer was 351 ± 3 nm.

Figure 7b shows the same sample after being annealed for two hours in the vacuum oven at 200 °C. The uniformity of the layer could not be increased, since the cracks still have the same size. The roughness of the annealed sample was even larger, at 6.3 ± 0.1 nm.

3.2.2 Titanium dioxide

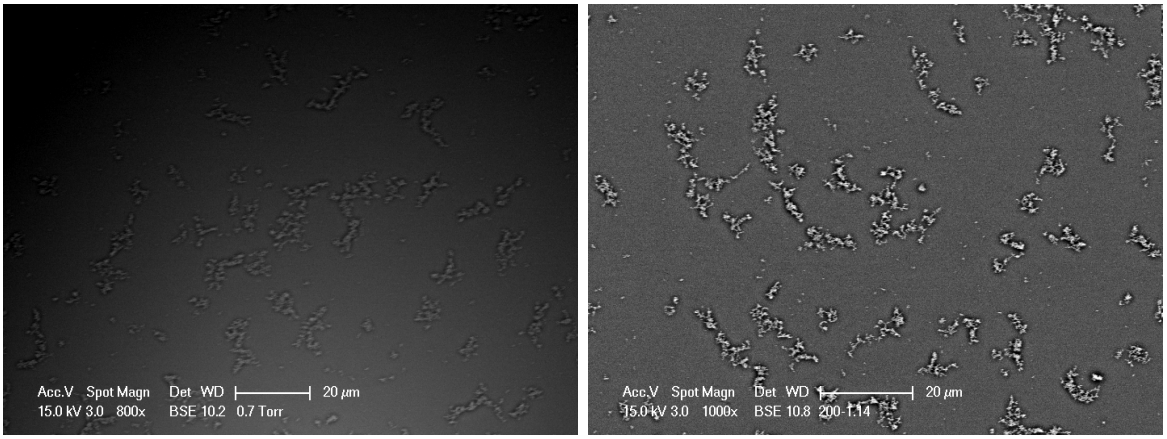

(a) Not annealed. (b) Hot Plate at 200 °C for 2h.

Figure 8: The titanium dioxide layers of Samples under the SEM. The sample on the right was annealed after the spin coating.

A titanium dioxide layer fabricated with sol-gel and spin coating methods is shown in Figure 8a. This sample gelled at 50°C for 15 minutes. The layer was not annealed after the spin coating. The titanium molecules on the wafer can be seen as lump-like structures with lengths of about 40 μm. These formed because the condensation reaction proceeded too quickly during gelification, therefore already forming solid xerogels before spin coating. During sol-gel these lump-structures deposited on the wafer, without a covering layer being

formed. Figure 8b shows the same sample after being annealed on the hot plate at 200°C for two hours. Also here the uniformity of the layer could not be improved, the layer still only consisted of single xerogel deposits.

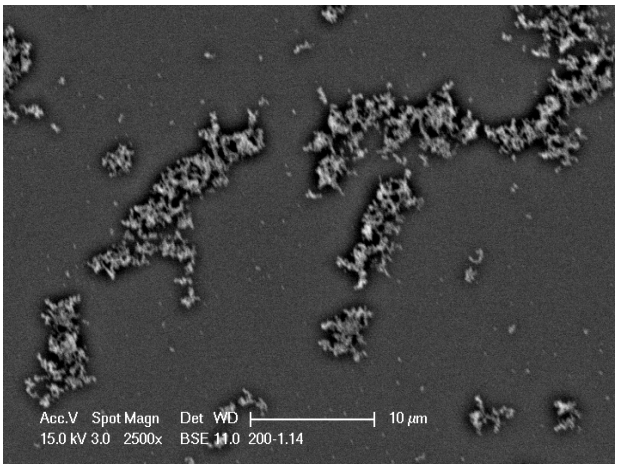

Figure 9: SEM picture of the titanium dioxide layer of Sample 3. It gelled at room temperature. This sample was not annealed.

Another sample (see Figure 9) was fabricated at a lower gelification temperature in order to have a slower condensation reaction and prevent the sol from gelling too fast before spin coating. However, also on this sample, only single xerogel deposits and not an evenly distributed layer formed.

3.2.3 Nanoparticles

The SEM images for Samples 5 and 6 are shown in Figure 10. Different concentrations of nanoparticles were added to a commercial sol-gel solution, in order to analyze the behaviour of the nanoparticles in these layers. They formed complexes with diameters up to 20 μm. These complexes were distributed throughout the whole samples and were well integrated in the layers. The sample with less nanoparticles added showed fewer cracks.

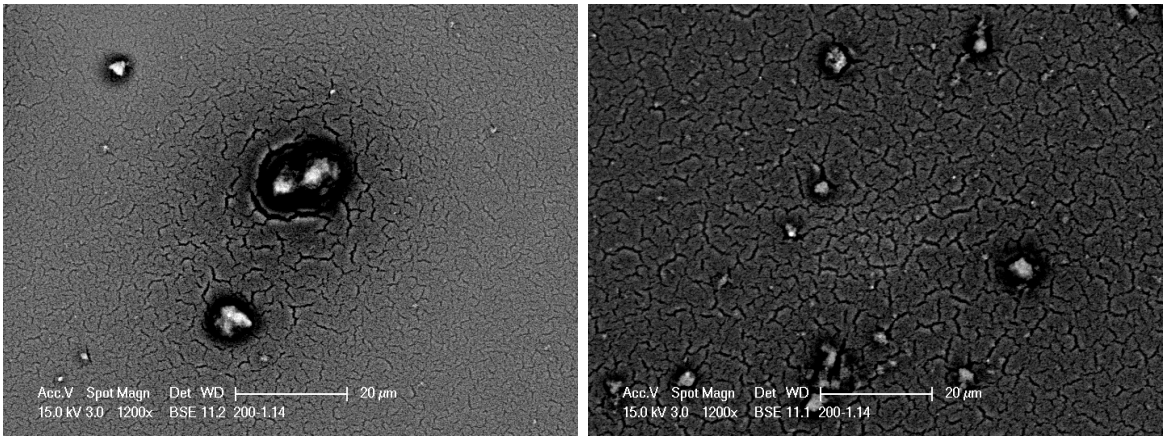

(a) 15 mg of nanoparticles added (b) 30 mg of nanoparticles added

Figure 10: SEM pictures of Samples 4 and 5 with aluminum nanoparticles. The precursor used for both samples was a commercial sol-gel solution. The nanoparticles formed complexes with a diameter up to $20\mu m$.

4 Discussion

4.1 UV Filter

The parameters for a UV filter that meets the stated requirements was achieved to have a peak transmissivity of 19.7 % at 200 nm and an average transmission of 1.6×10^{-10} $\pm$ 4.2×10^{-10}% for visible and infrared light. The extinction ratio at the upper boundary of the solar blind is around 4×10^{6}. This value could be increased by adding nanoparticles to the layers, which was not included in this model. The filtering of the light is mostly achieved by strongly reflecting the out-of-band wavelengths at the dielectric-metal transitions in the multilayer stack. Over 80% of the incident visible and infrared light is reflected.

The fundamental transmission characteristics of the filter were found to be conserved even when changing the angle of the incident light. A high transmission at 200 nm and a low transmission for longer wavelengths is given even for very large angles of incidence. Due to the longer propagation path of the light through the filter, absorption is increased and the peak transmissivity at 200 nm decreased to 9.7% for extreme angles, which is still sufficient.

A filter with the calculated parameters can definitely meet the requirement of wide acceptance angles.

The refractive index found for the stack of dielectric layers in the UV filter is 1.75. It lies between the refractive indices of silicon dioxide and titanium dioxide [5]. By mixing these materials in the right ratio, a dielectric material with the refractive index calculated in this study could be obtained. The optimized thicknesses of the filter, which vary from 31.7 nm to 47.6 nm for the dielectric layers and from 8.5 nm to 16.8 nm for the aluminum layers have to be made with extreme precision for the filter to meet the design specification of a $> 15\%$ transmission at 200 nm. If each layer of the filter is only 1 nm thicker, the peak transmission decreases to 3.8%. A variation to thinner layers has less influence on the performance of the filter, since the peak transmissivity $> 15\%$ at 200 nm is conserved and the transmission in the longer wavelengths only increases slightly.

The calculated values for the transmission and the reflection obtained from both MatLab and Lumerical are very close for values $> 10^{-5}\%$. However, the curves begin to diverge with smaller values (see Figure 4). The maximal difference between the two curves amounts to 4 orders of magnitude for wavelengths at 2,000 nm. This is due to rounding errors in the calculations. The disadvantage of the transfer-matrix method is that successively calculated values in the matrices have to be extremely precise in order for the final transmission values to be accurate. We reduced the rounding error by calculating the total inverse transmission matrix, in place of the regular transmission matrix that must be further translated into a scattering matrix to get the transmission. In this way a division of large numbers could be avoided and the accuracy of the calculations could be increased. Since the FDTD Method is less susceptible to rounding errors for small transmissions, the values obtained from Lumerical are more reliable for transmission values $< 10^{-5}\%$. The design specification of a transmission $< 10^{-9}\%$ for visible and infrared light was given in both curves.

4.2 Xerogel Layers

It is not realistic to obtain thicknesses accurate to within the range of less than 1 nm (see section 2.2.4) for a high performing UV filter with sol-gel and spin coating methods. The actual filter, therefore, has to be fabricated with chemical vapor deposition, sputtering or evaporation techniques. However, since nanoparticles cannot be inserted into the layers using these methods, an additional dielectric layer containing the aluminum nanoparticles fabricated with sol-gel and spin coating has to be added to the multilayer stack. The sol-gel and spin coating method seems applicable for this use. However, more uniform layers with less surface roughness have to be achieved.

The cracks in the silicon dioxide sample formed due to the fast evaporation of the water from the gel during spin coating. Annealing did not have a positive effect on the surface roughness. In the titanium dioxide samples solid xerogels formed during gelification due to the condensation reaction running too fast. Only single xerogel deposits and no covering layer formed during spin coating. Also the annealing of this sample did not increase the uniformity of the layer. The nanoparticles inserted into the sol did not distribute evenly, but formed large complexes with sizes up to 20 μm. This was the case since the surfaces of the nanoparticles were not charged in the sol. The van der Waals attraction force therfore dominated over the electrostatic repulsion and the nanoparticles aggregated [11]. By increasing the pH of the sol, the surface charge of the nanoparticles is increased, thereby repelling each others and becoming evenly distributed in the layer. Since the pH also has an influence on the structural properties of the forming gel layer, the value giving both a uniform layer and evenly distributed nanoparticles needs to be found.

5 Future Work

The structural propeties of the xerogel layers need to be enhanced to have more uniform layers. The number of cracks in the silicon dioxide layers may be decreased by lowering the acceleration of the gel during spin coating. In this way the evaporation could take place more slowly, which would result in fewer cracks in the layer. For the titanium dioxide layers, the speed of the condensation reaction should be decreased. This may be realized by lowering the concentration of titanium isopropoxide in the sol, further lowering of the temperature during gelification or using the pH value to control the reaction speed. The effect of the pH on the structural properties of the film and on the distribution of the nanoparticles has to be studied simultaneously. By increasing the pH, the surface charge of the nanoparticles and therefore their distribution in the layer due to repulsive forces could be obtained.

6 Conclusion

The parameters for a UV filter with a peak transmission of $\sim$20% at 200 nm and a transmission lower than 10^{-9}% in the visible and infrared spectrum were successfully optimized in an extensive computer simulation. According to the results obtained from two independent simulations the filter accepts a wide range of angles of incidence. In order to get a high performance, the thicknesses of the dielectric and aluminum layers should vary less than 1 nm from the values calculated in this study. The fabrication of these layers using sol-gel and spin coating techniques is not realistic, since they are very sensitive to small changes in parameters, making it difficult to fabricate a uniform and smooth layer. However, a xerogel layer additional to the multilayer stack could be added, containing the nanoparticles for the enhancement in the extinction ratio at the upper boundary of the solar blind. In order to create uniform layers, a high pH is needed so that the nanoparticles are charged, repulsing each other and becoming evenly spread within the layer.

7 Acknowledgments

I would like to thank my mentors, PhD candidates Mr. Corentin Monmeyran and Mr. Brian Pearson, for helping me with my project and introducing me to scientific research. I would like to express my gratitude to Dr. Anuradha Agarwal and the other staff of the Electronic Materials Research Group led by Prof. Lionel C. Kimerling at the MIT Center for Materials Science and Engineering (DMSE), for letting me become a part of the team. The SEM and profilometer results would not have been possible without the staff of the Electron Microscopy and the Materials Analysis at MIT DMSE. I would like to thank Ms. Marie Herring and Ms. Ava E. Chen for helping me to write my paper and continually giving me advice. I would further like to acknowledge the Massachusetts Institute of Technology (MIT), the Center for Excellence in Education (CEE), and the Research Science Institute (RSI). Last but not least, I would like to express my gratitude to Ms. Beatrice Giovannoni, president of the Association for the promotion of Especially Gifted Children, and Dr. Frank Ziemer, president of Ziemer Ophthalmic Systems AG, for giving me the possibility to participate in RSI.

References

[1] Z. Xu, H. Ding, B. M. Sadler, and G. Chen. Analytical performance study of solar blind non-line-of-sight ultraviolet short-range communication links. *Opt. Lett.*, 33(16):1860–1862, Aug 2008.

[2] G. C. Z. Xu and M. L. F. Abou-Galala. Experimantal performance evaluation of non-line-of-sight ultraviolet communication systems. 2007.

[3] T. Erdogan and A. Pradhan. Optical filters go deeper. *Photonics Spectra*, 42(3):76, 2008.

[4] E. X. Prez. *Design, Fabrication and Characterization of Porous Silicon Multilayer Devices*. Universitt Rovira I Virgili, 2007.

[5] M. Polyanskiy. Refractive index database, July 2014. Available under http://refractiveindex.info/.

[6] B. E. A. Saleh, J. Wiley, and I. Sons. *Fundamentals of Photonics (Second Edition) Bahaa E. A. Saleh, Malvin Carl Teich. [electronic resource] /.* Wiley-Interscience, 1st ed edition, 1991. Electronic reproduction. Somerset, New Jersey : Wiley InterScience, 2001. Available via World Wide Web.

[7] R. F. Bunshah. Handbook of deposition technologies for films and coatings. 2:83, 1994.

[8] S. Abedrabbo, B. Lahlouh, S. Shet, A. Fiory, and N. Ravindra. Spin-Coated Erbium-Doped Silica Sol-Gel Films on Silicon. *ArXiv e-prints*, Feb. 2012.

[9] C. Brinker and G. Scherer. *Sol-gel Science: The Physics and Chemistry of Sol-gel Processing*. Academic Press, 1990.

[10] Surface roughness measurement. *Mitutoyo*, (1984), 2009.

[11] H. M. S. Gosh, P. B. B. Pan, and B. Xing. Colloidal behavior of aluminum oxide nanoparticles as affected by ph and natural organic matter. 2008.

III Nachwort

Endlich spürte ich wieder Optimismus in mir aufkommen, das Gefühl, dass alles gut kommt. Dies war in der vierten RSI-Woche. Die Woche davor hatte mein MatLab-Programm, das die Licht-Transmission des Filters als Funktion der Wellenlänge darstellen sollte, Prozentzahlen von mehreren Hundert Zehnerordnungen geliefert. Dass das nicht sein kann, war offensichtlich. Aber wo lag das Problem? Physikalisch stimme meine Matritzenrechnung, hatte mir einer meiner Mentoren nach Kontrolle meines Programmcodes versichert. Nun musste ich selber zunächst das Problem und dann auch noch eine Lösung dafür finden. Den entscheidenden Hinweis lieferte mir schliesslich einer aus dem Team, mit dem ich mich während der Teamsitzung unterhielt: Er hatte in einem sehr ähnlichen Fall auch völlig falsche Zahlen von seinem Programm geliefert erhalten. Das Problem sei damals eine ungenügende Anzahl an signifikanten Stellen in der Berechnung von MatLab gewesen. Bei so vielen multiplizierten Matritzen braucht es im einzelnen Rechnungsschritt nur eine kleine Ungenauigkeit, um das Endprodukt enorm von seinem eigentlichen Wert abweichen zu lassen. Schliesslich fand ich in der Arbeit „Design, Fabrication and Characterization of Porous Silicon Multilayer Devices" [4] die Lösung für diese Rundungsungenauigkeit: Mit dem Rechnungsweg über die totale inverse Matrix (wie im Kaptiel 2.1.1. beschrieben) kann am Schluss die Division von zwei sehr grossen Zahlen umgangen werden, wodurch die Genauigkeit des Resultats stark verbessert wird. Ich erklärte meinen Lösungsweg meinem Mentor, drückte mich aber in der Euphorie wohl nicht klar genug aus. Ganz ruhig zeichnete er sodann die römischen Ziffern von eins bis vier auf das von meinen Erklärungsversuchen vollgekritzelte Blatt. „Is there something special about these numbers?", fragte er mich. Mit dem Kopf noch bei der totalen inversen Matrix überraschte mich diese Frage. „The first three numbers are just lines. The number one has one line, the number three three", fuhr er fort. „But four is different. It consists just of two signs. And this makes sense. The human brain is not used to understand more than three things at the time. You were explaining your concept with about six ideas. Be more precise!"

Dies ist nur ein kleines Beispiel der Dinge, die ich während RSI gelernt habe und die mir in Erinnerung geblieben sind. In Bezug auf das selbständige wissenschaftliche Arbeiten habe ich sicher grosse Fortschritte gemacht.

Hätte ich eine Maturaarbeit in der Schweiz geschrieben, hätte ich mich wohl enger an die Richtlinien des Gymnasiums halten können als in den USA; wo ich die dort geltenden Regeln zu befolgen hatte. Beispielsweise das Ausarbeiten einer geeigneten Fragestellung. Dies wurde in meinem Fall von meinen Mentoren gemacht, die mit der einzigen Auflage, dass in den rund vier Wochen für einen Gymnasiasten ein gutes Resultat herausschauen sollte, mein Projekt bestimmten. Dafür konnte ich in anderen Bereichen Erfahrungen sammeln, die ohne RSI nicht möglich gewesen wären. Ich möchte die wichtigsten drei hier kurz wiedergeben.

I. Jeden Entscheid gut begründen können

Obwohl dieser Punkt eigentlich trivial ist, hatte ich zu Beginn meiner Forschungsarbeit Mühe damit. Immer, wenn ich meinen Mentoren über den Stand des Projektes berichten musste, beharrten sie auf klaren und präzisen Begründungen. Einmal wählte ich beispielsweise bei der Optimierung der Parameter (Table 1) 100 nm als Oberwert für die Dicken, was zum Glück funktionierte, da Multilayer-Strukturen grundsätzlich mit Dicken arbeiten, die nur einen kleinen Bruchteil der Wellenlänge des Lichtes messen, für das der Filter entwickelt werden sollte (in meinem Fall 200 nm). Ich hatte für diese Wahl jedoch keinen stichhaltigen Grund und so hätte es auch schlecht herauskommen können. Dieser Punkt ist in der Forschung sehr wichtig.

II. Mit Unvorhergesehenem umgehen können

Selbst am MIT, oder vielleicht gerade besonders am MIT, wo viele sehr hoch entwickelte Forschungseinrichtungen vorhanden sind, kommt es immer wieder zu Defekten. So fiel in der ganzen dritten Woche die Pumpe für das destillierte Wasser aus (gerade dann, als ich es verwenden wollte) und in der Woche darauf funktionierte das Elektronenmikroskop nicht mehr (als meine Teststücke für die Analyse bereitgelegen hätten). Mit einer Maturaarbeit, deren Verlauf besser absehbar gewesen wäre, hätte ich vermutlich besser geschlafen. Aber es ist ja nicht zuletzt auch dieses Unbekannte und Unvorhersehbare, das die Forschung spannend macht. Niemand weiss genau, wohin die Reise geht. „Research shouldn't be the only thing in your life", sagte einmal einer der Mentoren zu mir, „otherwise you suffer too much if there is no progress."

III. Sich im Team austauschen

Zu Beginn mochte ich die Sitzungen im Forschungsteam nicht. Ich konnte nicht wirklich mitreden, da ich die Projekte der anderen nur der Spur nach verstand. Viel lieber wollte ich mit meinem Projekt, das mir zeitweise Sorgen bereitete, vorwärts kommen. Warum sollte ich also immer bei den Sitzungen anwesend sein? Meine Mentoren bestanden darauf, und ich wagte natürlich nicht, mich zu widersetzen. Schliesslich war es aber während einer solchen Sitzung, dass mir einer aus dem Team den Hinweis mit den Rundungsfehlern im MatLab-Programm gab. Im Rückblick muss ich meinen Mentoren Recht geben. Obwohl alle an einem anderen Projekt arbeiten, ist es wichtig, dass man sich austauscht. So bekommt man etwas Distanz zu den eigenen Problemen, merkt, wo es noch Fehler geben könnte (kann man seine Entscheide hinreichend begründen?) und wird auf neue Ideen gebracht. Ein Wissenschaftler als Einzelkämpfer hat sicher keine Zukunft.

Ich habe während RSI und dieser Maturaarbeit sehr viel über die Wissenschaft, die Forschung und die verschiedenen Arbeitsprozesse einer solchen Arbeit gelernt. Das Durchführen und Niederschreiben meines Projektes fielen mir nicht leicht und es kam gegen Ende sogar zu schlaffreien Arbeitsnächten, um alles rechtzeitig in den sechs Wochen von RSI zu schaffen. Ich bin aber stolz auf das vorliegende Produkt und hoffe, dass es interessant zu lesen ist.

IV Danksagung

Ich möchte Dr. Christoph Rytz für seinen Einsatz vor und während des Research Science Institutes und in der Entstehung dieser Arbeit ganz herzlich danken. Ohne ihn wäre meine Teilnahme am RSI nicht möglich gewesen. Weiter möchte ich meinen Dank für die Schulleitung und das Lehrerkollegium der Abteilung MN am Gymnasium Kirchenfeld aussprechen, die meine Pläne unterstützt und mitgeholfen haben.